ADAPTIVE GRID REFINEMENT FOR CONVERGENCE STUDIES

Jeroen Wackers, Ganbo Deng, Emmanuel Guilmineau, Alban Leroyer, Patrick Queutey, Michel Visonneau

6th European Conference on Computational Mechanics (ECCM 6)
7th European Conference on Computational Fluid Dynamics (ECFD 7)
1115 June 2018, Glasgow, UK

ADAPTIVE GRID REFINEMENT FOR CONVERGENCE STUDIES

JEROEN WACKERS, GANBO DENG, EMMANUEL GUILMINEAU, ALBAN LEROYER, PATRICK QUEUTEY AND MICHEL VISONNEAU

LHEEA, UMR-CNRS 6598, Ecole Centrale de Nantes
1 rue de la Noë, B.P. 92101, 44321 Nantes cedex 3, France
jeroen.wackers@ec-nantes.fr, https://lheea.ec-nantes.fr

Key words: Adaptive Grid Refinement, Grid Convergence Studies, Nested Grids

Abstract. Adaptive refinement of unstructured hexahedral meshes is used to produce series of nested grids. Tests show that these series can be used in grid convergence studies, to estimate numerical uncertainties in computed forces and to study local flow features.

1 INTRODUCTION

Numerical simulation of fluid flow for today's practical applications often involves the use of unstructured grids. Modern unstructured grid generators allow the simulation of complex geometries, while they can perform the mesh generation in an industrial context largely automatically. Unfortunately, most unstructured mesh generators cannot precisely control the local cell sizes and orientations throughout the mesh, which makes it difficult to generate series of coarse to fine meshes where the ratios of the cell sizes are the same throughout the mesh (so-called conformal or nested meshes). As such series of meshes are needed for verification studies, this difficulty is one of the main bottlenecks for the widespread adoption of verification on unstructured meshes.

We have recently shown [1] that adaptive grid refinement can create series of nested unstructured grids, provided that the refinement is based on a metric criterion. Adaptive refinement is the technique of locally refining an initial coarse grid by subdivision of the cells, based on a refinement criterion which indicates where the flow needs a better resolution. In the metric context, this criterion is a real field computed from the flow; the mesh is refined such that the product of the local cell size and the criterion everywhere is equal to a constant threshold value. Thus, if the criterion varies little when the mesh is refined, all the cell sizes are proportional to this threshold. This implies that series of meshes can be created by starting adaptive refinement from the same initial mesh and simply varying the threshold value.

These simulations and grid refinement are performed with the ISIS-CFD unstructured finite-volume incompressible RANS solver developed by the authors. This code is used for the realistic simulation of industrial-type flows, it is available as the flow solver of the FINE™/Marine computing suite. Its adaptation method is based on the refinement

of unstructured hexahedral grids by subdivision of the cells [2]. Anisotropic refinement, where the cells are adapted to the flow both in size and in aspect ratio, is handled with the metric tensor approach introduced by George and Borouchaki [3], modified for the refinement of hexahedrals.

This paper is a summary of [1]. It presents series of grids that are created for two test cases: a two-dimensional airfoil and a ship, the KVLCC2 tanker. The meshes are studied to ascertain that they have the characteristics of nested grids. An established uncertainty estimation method [4] is then applied to the computed series of forces, to see if useful estimations are produced. Finally, visual inspection of the wakes is used to find out if the local flow field can be brought close to grid independence.

2 FLOW SOLVER AND ADAPTIVE REFINEMENT

ISIS-CFD is an incompressible unsteady multifluid Navier-Stokes solver [5, 6]. This section introduces the solver and its adaptive grid refinement method.

2.1 Discretisation and physical models

The solver is based on the finite volume method to build the spatial discretisation of the transport equations. Pressure-velocity coupling is obtained through a Rhie & Chow SIMPLE-type method. The discretisation is face-based, so cells with an arbitrary number of arbitrarily-shaped faces are accepted; most computations are performed on unstructured hexahedral meshes. The code is fully parallel using the MPI (Message Passing Interface) protocol.

Turbulence is principally modelled with the Reynolds-averaged Navier-Stokes (RANS) equations and advanced turbulence closures, such as the anisotropic EASM model [5]. Furthermore, several Detached-Eddy Simulation (DES) models are available. If a free surface is present, it is captured with a mixture-model approach [6]. For brevity, the other solver options are not described here.

2.2 Grid refinement method

The adaptive grid refinement technique in ISIS-CFD performs isotropic and anisotropic refinement of unstructured hexahedral meshes. Adapted meshes are created by dividing the cells of a coarse original grid into finer cells; this division can be repeated several times until the desired cell sizes are obtained. Anisotropy is introduced by splitting cells in one direction only. The mesh is adapted regularly during the computation in order to follow the convergence of the flow; earlier refinements can be undone to account for the changes in the flow as it converges.

To obtain anisotropic grid refinement, we use metric tensors as refinement criteria. This technique was introduced for the generation of anisotropic tetrahedral cells [3], it also provides a practical and flexible framework for the refinement of hexahedral meshes. The refinement of the cells is decided as follows. First, the 3×3 criterion tensors $\mathcal{C}_i$ in each cell i are computed (in some way) from the flow solution. In a hexahedral cell, let the cell sizes $\mathbf{d}_{i,j}$ $(j = 1, 2, 3)$ be the vectors between the opposing face centres in the three

cell directions. The goal of the grid refinement is then to create a grid which is uniform under the transformation $\mathcal{C}$, which implies that:

$$\|\mathcal{C}_i \mathbf{d}_{i,j}\| = T_r \qquad \forall i, j, \tag{1}$$

where T_r is a constant. This is accomplished by refining cells i in the direction j, until $\|\mathcal{C}_i \mathbf{d}_{i,j}\|$ no longer exceeds the constant T_r. Equation (1) implies that the tensors $\mathcal{C}$ are direct specifications of the desired cell sizes: in a converged refined grid, the cell sizes are inversely proportional to the magnitude of the $\mathcal{C}$.

The refinement criteria are based on the Hessian matrix of second spatial derivatives. To adapt the mesh to pressure-based flows but also to boundary layers, wakes, and shear layers, a criterion is chosen based on the Hessians of both the pressure and the velocity [1]. To give equal importance to the different Hessian matrices, they are weighted in the way in which they appear in the flux.

3 USING GRID REFINEMENT FOR CONVERGENCE STUDIES

To allow extrapolation towards the grid-independent solution, grid convergence studies require a series of computations on different meshes for which the local truncation errors vary proportionally to a single global mesh size parameter. Since truncation errors in general depend on the shapes and orientations of the cells as well as on their size, such meshes need to have cells of similar shape in any given position and the ratio of the cell sizes between two meshes must be constant throughout the mesh (see for example [4]).

Metric-based anisotropic grid refinement methods such as the one outlined in section 2.2 can create series of geometrically similar unstructured meshes naturally. Thanks to the use of metric tensors, the threshold T_r globally specifies the fineness of the grid: if the refinement criterion remains constant as the mesh is refined, the mesh size everywhere is proportional to T_r (equation 1). Furthermore, the refined grids are created by cell division, so the refined cells conserve the shape and orientation of the cells in the original grid. Thus, two meshes refined from the same original grid have similar cell shapes. This means that series of geometrically similar meshes can be created by starting from the same original grid and simply varying T_r.

A limitation of this approach is that the refinement procedure cuts cells in half, so the cell sizes in the original grid can only be reduced by a power of two. Thus, if T_r is reduced by anything other than a power of two between subsequent meshes, the cell sizes are divided by the nearest power of two and the zones with cells of the same size become larger or smaller (see figure 6 for an example). While such meshes still resemble each other closely, they are not formally geometrically equivalent.

Furthermore, the mesh size is not proportional to T_r in those regions where the original grid is not refined at all. To obtain grids that are similar in these zones, one could make a different original grid for each threshold. However, if such grids are unstructured, they are rarely exactly similar close to the walls, where the grid is deformed to follow the walls. Thus, to improve the similarity in the unrefined parts of the mesh which are by definition the least interesting for the flow, one would reduce the similarity in the most critical

parts of the mesh, the near-wall regions. Therefore, we base our convergence studies on the same original mesh for all grids.

4 NAKAYAMA B TWO-DIMENSIONAL AIRFOIL

A first test of the proposed method is performed on a two-dimensional case. On two different series of meshes, the convergence of the global forces and the related uncertainty estimation is studied, as well as the grid-independence of the local flow.

4.1 Test case, computations and meshes

The test case is the Nakayama B airfoil, for which measurements of the velocity and the turbulence intensity have been performed both in the boundary layers and in the wake [7]. The airfoil is a supercritical profile with chord $c = 61$ cm, placed at $\alpha = 4^o$ in the centre of a 137 cm high test section. The flow is incompressible with $Re = 1.2 \cdot 10^6$. Simulations are performed with the $k - \omega$ SST turbulence model.

The first series of meshes has a low-Reynolds (no-slip) boundary condition on the airfoil. The original mesh for these computations has 5755 cells and $y^+ \approx 1$ on the walls. A second series is created with a wall-law boundary condition, for which the original grid has 2623 cells and $y^+ \approx 30$. All series consist of ten meshes. For each mesh, the refinement threshold T_r is divided by $\sqrt{2}$ with respect to the previous mesh (thus, the cell sizes are halved every two meshes). The T_r go from 0.5000 to 0.0221.

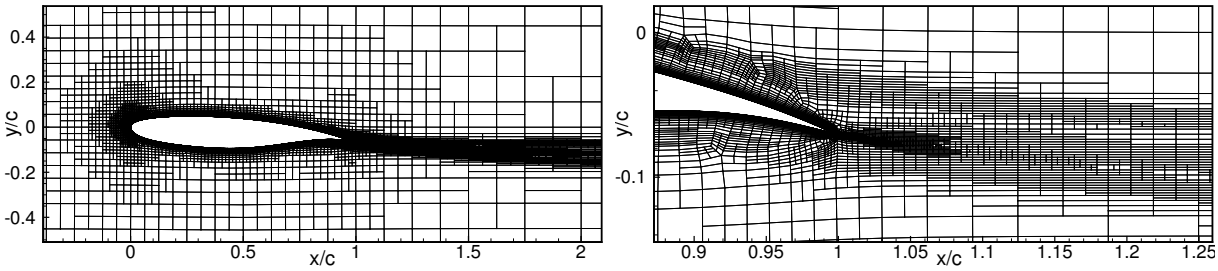

Figure 1: Refined mesh for the Nakayama airfoil with $T_r = 0.125$ and low-Reynolds wall boundary condition. The right figure shows a close-up around the trailing edge.

Figure 1 shows the adaptively refined mesh with low-Reynolds boundary conditions and $T_r = 0.125$. The mesh is refined around the pressure peak at the leading edge, as well as in the boundary layer and wake. Concentrations of fine cells are found near the outside of the wake, where the second derivatives of the velocities are high.

A detail of the meshes in figure 2 shows the grid convergence for three thresholds. This figure confirms that as the threshold is halved, the refined cells become twice smaller. The zones of fine cells have the same shape in the three figures and even though the refinement is mostly isotropic, the small zones of anisotropic refinement between the cells with different sizes are roughly similar. Furthermore, since these meshes come from the same original grid, the orientations of the cells are identical. If this is enough for convergence studies, will be seen below.

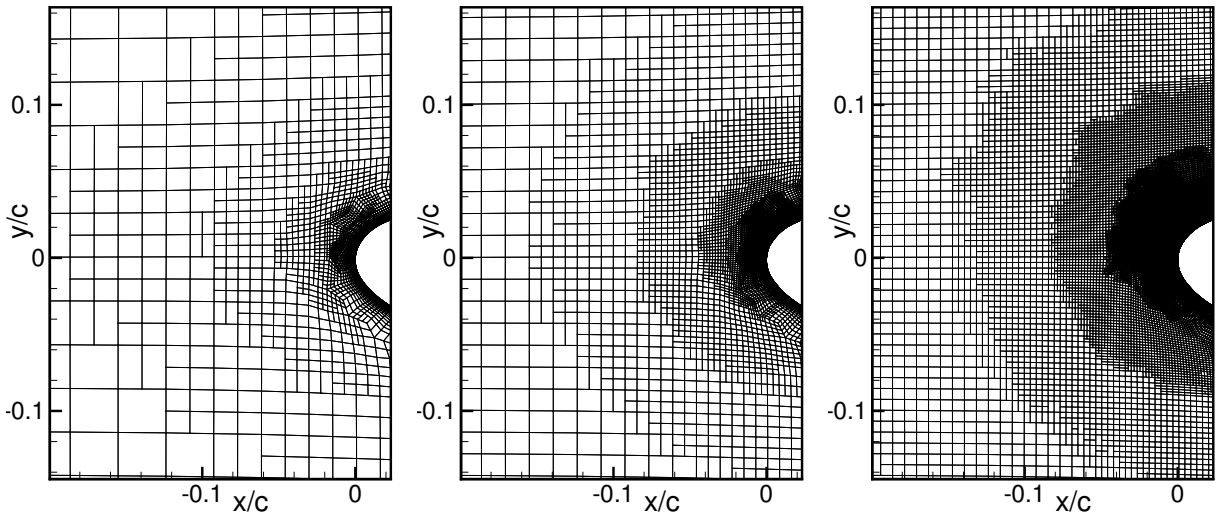

Figure 2: A detail of the low-Reynolds meshes, for progressively finer thresholds. Left to right: $T_r = 0.125$, $T_r = 0.0625$, and $T_r = 0.0313$.

4.1.1 Estimated uncertainties

For all computations, the convergence of the force coefficients $C_d = F_x/(\frac{1}{2}\rho V^2 cb)$ and $C_l = F_y/(\frac{1}{2}\rho V^2 cb)$ is studied, where the forces are computed on a wing segment of unit span $b = 1$. Uncertainty estimations are performed following Eça and Hoekstra [4].

The dependence of C_d and C_l on T_r is shown in figure 3; starting from the third grid, estimated uncertainties are included. To resemble the usual type of convergence study where a large number of grids is not available, the uncertainties on each grid are computed from not more than five grids: the grid itself and the previous four, if these exist.

The low-Reynolds grids provide the most complete simulation of the flow, since the wake and the boundary layer are fully resolved. Figure 3a shows a convergence for C_d that appears asymptotic with some superimposed high-frequency noise. The uncertainty estimation works well here: all the uncertainty intervals contain the actual converged C_d and those computed with five or four grids ($T_r \leq 0.1768$) are not excessively large. For C_l, even on the coarsest grids, the computed values are close to the solution on the finest grid. Unfortunately, this means that the convergence is dominated by noise so the estimated uncertainties are high; the estimation cannot show how good the coarse-grid solutions really are. Realistic error bars are obtained for $T_r \leq 0.0625$.

Similar results are obtained for the wall law series (figure 3b), so the use of the wall law does not perturb the grid convergence. However, this boundary condition introduces a modelling error so the two series do not converge to the same value for C_d. For the thresholds $T_r \leq 0.0625$, the uncertainty intervals for C_d do not overlap between the low-Reynolds and the wall law series. Thus, the two series can be used to compute the modelling error reliably.

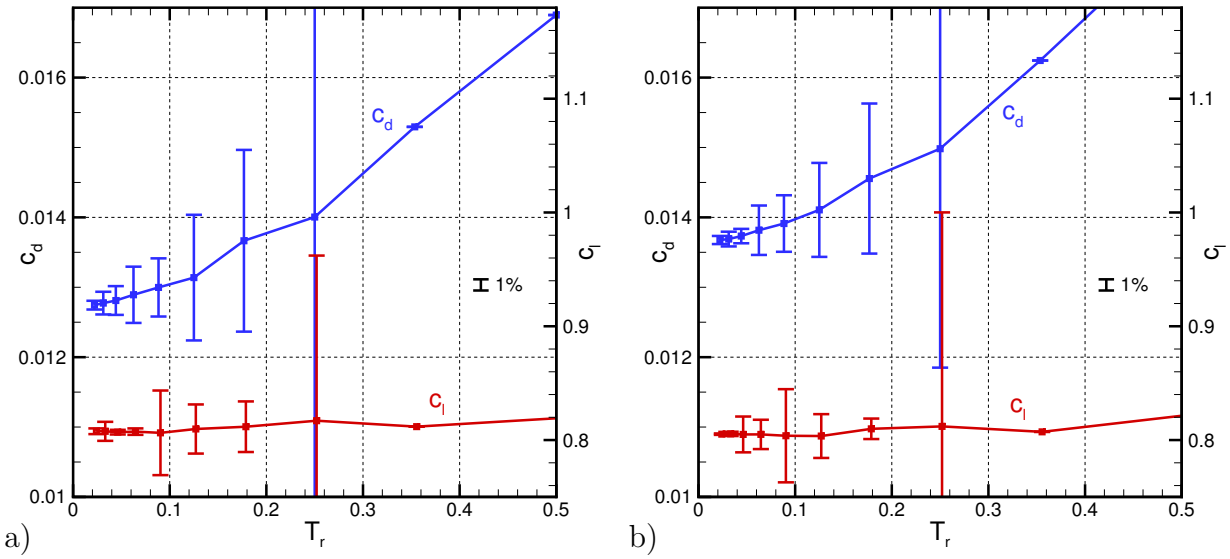

Figure 3: Convergence of drag coefficient C_d and lift coefficient C_l for the Nakayama airfoil, with respect to the threshold T_r. Low-Reynolds grid (a) and wall-law grid (b). The two vertical axes are scaled such that error bars of the same length for C_d and for C_l indicate the same relative uncertainty.

4.2 Grid-independence of the local flow

Much of the interest of grid adaptation is in the precise computation of local flow details. Therefore, this section studies the grid convergence of the near and far wake. Figure 4 gives the velocity and one component of the turbulent fluctuation for the two series. Judging visually from the distance between the curves, on the $T_r = 0.0442$ grid the solution is converged, the $T_r = 0.0884$ grid is close, and the $T_r = 0.1768$ grid already gives the right tendencies.

The results are not the same for low-Reynolds and wall-law boundary conditions. The most notable effect of the wall law is the attenuation of the turbulence peak at the trailing edge in the near wake, which corresponds to the position where the grids differ most (figures 1b and c). However, even in the far wake a reduction in the velocity defect and the turbulence intensity can be seen due to the wall law.

Compared with the experiments [7], the shape of the turbulence profiles is well captured in both cases but the intensity is too low, so the wake and the boundary layer are too thin. Also, unlike the experiments, the edges of the wake are sharp in the numerical solutions. This is only observed because of the extra-fine grid around the edge of the wake (figure 1b); on coarser refined grids and therefore on standard boundary layer grids also, the numerical solution is closer to the experiments. This modelling error is therefore only visible thanks to the adaptive refinement.

Thus, from the $T_r = 0.0884$ grids on, the differences between the solutions in one series are small compared with the difference between low-Reynolds and wall-law solutions. Both these differences are small with respect to the distance between the simulations and the experiments. Thus, the $T_r = 0.0884$ grid and all finer grids indicate modelling errors in the wake reliably.

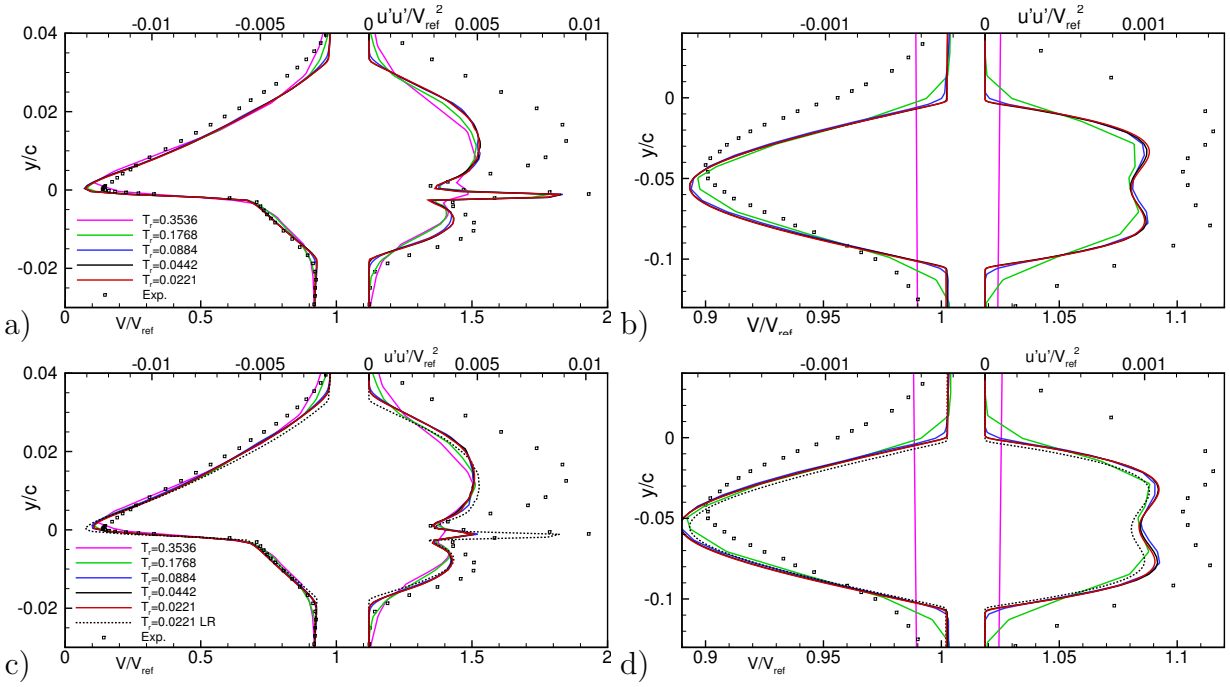

Figure 4: Velocity V (left lines) and fluctuation correlation $\overline{u'u'}$ (right lines) in the wake of the Nakayama airfoil, at $0.01c$ (a, c) and $2.0c$ (b, d) behind the trailing edge. Low-Reynolds boundary conditions (a, b) and wall law (c, d).

5 KVLCC2 TANKER

The flow around the KVLCC2 tanker ship has a complex aftbody flow with boundary layer separation and different vortical structures; figure 5 gives a global view of the flow field, with the thickening and separation of the boundary layer.

The flow is computed for a model of the ship with length $L = 5.571m$, which gives $Re = 4.6 \cdot 10^6$. Since the flow is symmetric, only half the hull is simulated. Free-surface effects are ignored: the water surface is treated as a symmetry plane, like the vertical centreplane. Larsson et al. [8] give a complete description of the test case.

The flow is simulated here with a wall law approach and the anisotropic EASM turbulence model including rotation correction, since this model represents flows dominated by longitudinal vorticity better than the standard $k - \omega$ SST model [5]. Convective terms are discretised with a blended central / upwind scheme.

5.1 Refined meshes

For the convergence study five different thresholds are used (table 1), with a factor 4 between the cell sizes of the coarsest and finest mesh. The refined meshes in the propeller plane (the aftmost cut plane on the hull in figure 5) are shown in figure 6 for the four finest thresholds. These meshes are refined around the principal features of the flow, such as the main aft-body vortex whose centre is near (0.01, -0.04). This vortex creates an open-type separation on the hull, with an associated ear-shaped shear layer that is captured with fine cells. A second shear layer starting at (0.0, -0.065) separates the boundary layer flow

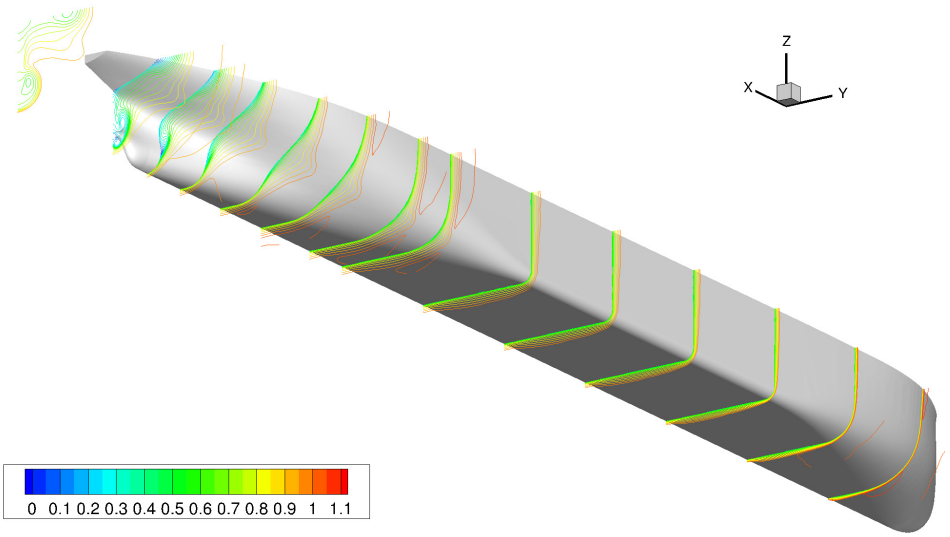

Figure 5: KVLCC2: the (half) hull and the axial velocity field.

around the vortex from the flow outside. Like for the 2D wing, the outer edge of the boundary layer attracts grid refinement.

Table 1: KVLCC2: thresholds and mesh sizes.

T_r	3.0	2.0	1.5	1.0	0.75
nb. cells	247k	613k	1.34M	5.02M	10.18M

The geometric similarity of the grids is shown by figures 6a and c, as well as b and d. The thresholds for these images differ by a factor two, so cells should be twice smaller in each second image. This is mostly the case; the centre of the vortex with its vertically elongated cells is an example. However, there is a perturbing effect here that was not encountered before: as the mesh is refined, the flow field changes so the refinement criterion is modified, which leads to non-similar meshes. This effect is stronger than for the 2D case, because the KVLCC2 flow has more shear layers and discontinuities in the velocity gradients, which become sharper on fine meshes. Thus, especially on the outer edge of the boundary the grid size decreases more than linearly with T_r. This is not necessarily a problem, since the sharp resolution of these features improves the quality of the local flow on the fine meshes, while globally seen the four grids form a reasonable series.

5.2 Convergence of the flow

The convergence of the resistance force $C_T = F_x/(\frac{1}{2}\rho V^2 S)$, with $S = 0.2682L^2$, is monotone (figure 7a). Numerical uncertainties were again estimated with the method of Eça & Hoekstra. The error bars computed with 3, 4 and 5 grids overlap, which is an indication that the procedure works well. On the finest grid, the uncertainty is 1.69%.

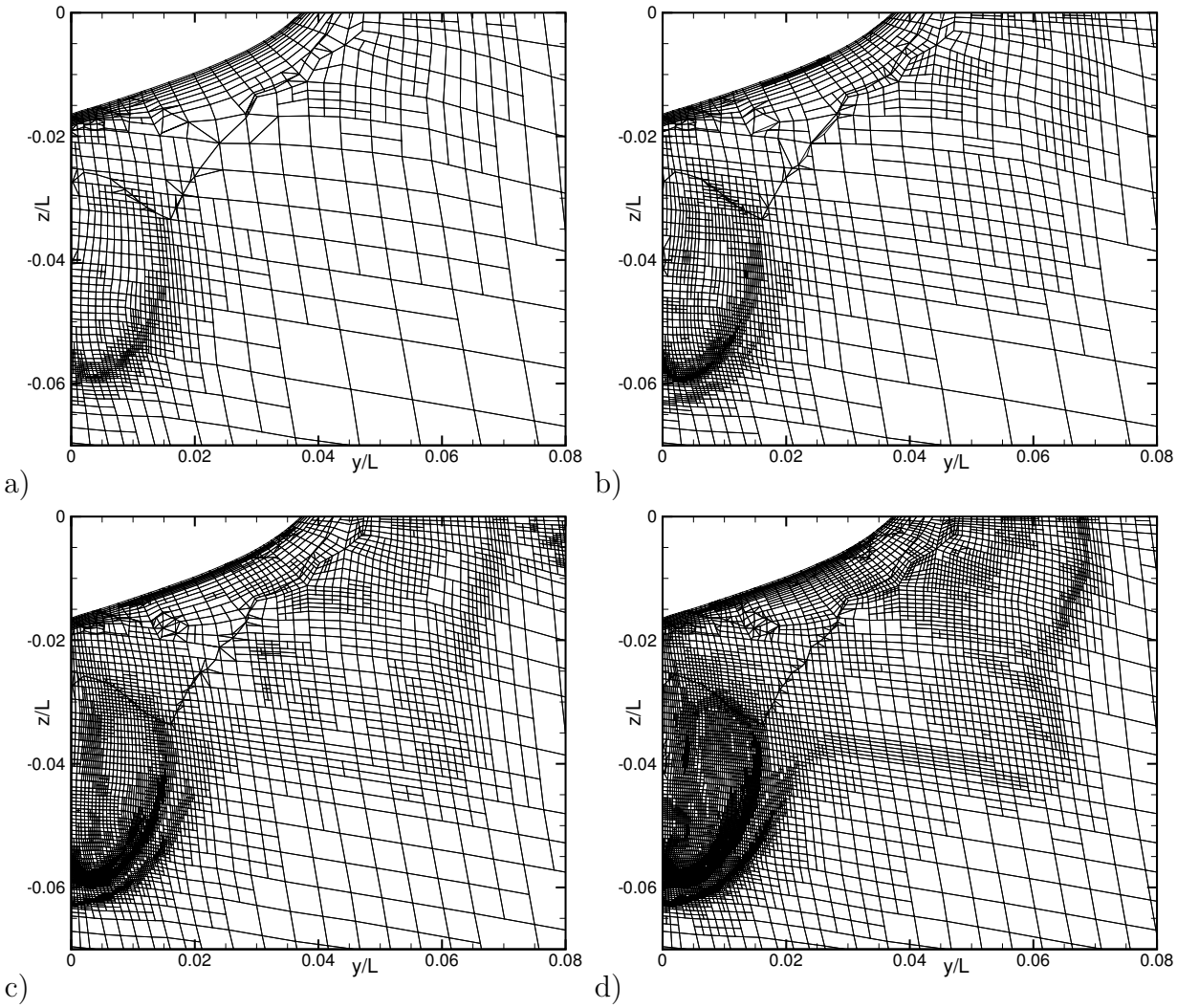

Figure 6: Meshes in the propeller plane $x/L = 0.9825$ of the KVLCC2, $T_r = 2.0$ (a), $T_r = 1.5$ (b), $T_r = 1.0$ (c), and $T_r = 0.75$ (d).

However, more noise is present than for the Nakayama case, which may be due to the irregularities in the mesh noted above. Due to the complexity of the case, it is also possible that a higher-order error is present.

The convergence of the pressure force coefficient C_{Tp} and the viscous force coefficient C_{Tv} are given in figures 7b and 7c respectively. While the viscous force is about four times larger than the pressure force, their variation across the grids and the computed uncertainties are of the same magnitude. Both figures show that the forces are not in the asymptotic range, but the estimated uncertainties are reasonable, especially for the viscous forces where the uncertainty intervals overlap. The pressure force has some more irregularity. The estimated uncertainties are 6.47% for C_{Tp} and 1.11% for C_{Tv}.

The grid convergence of the local flow is good (figure 8). Even though the overlapping isolines of the Nakayama case are not obtained, the velocity and turbulence isolines for the

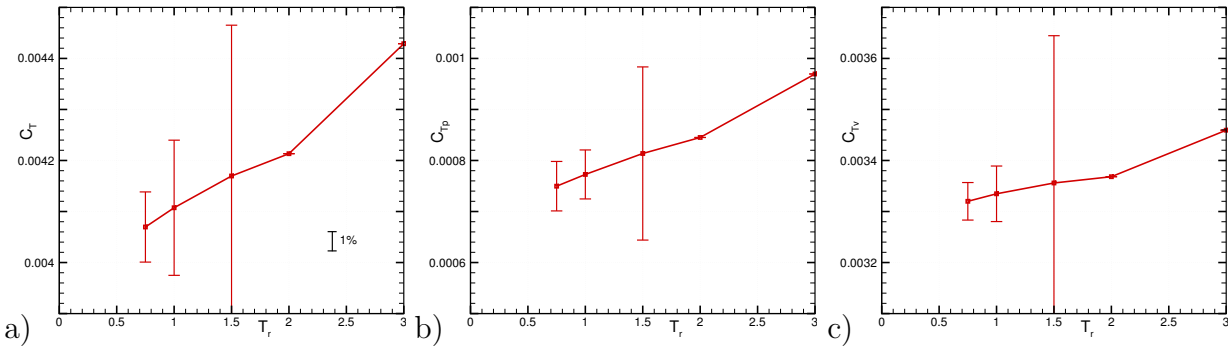

Figure 7: Grid convergence for the KVLCC2: resistance coefficient C_T (a), pressure and viscous resistance coefficients C_{Tp} (b) and C_{Tv} (c), with uncertainty computed using all the coarser grids available. The scale of the axes is the same for the three graphs.

finest grids are very close throughout the aft-body flow and also in the near wake. Even the 0.9 axial velocity isoline which represents the outer boundary layer, often underresolved in KVLCC2 simulations, is close to convergence thanks to the adaptive refinement. And finally, the differences between the two finest meshes are small compared to their difference with the wind-tunnel measurements from KRISO. Thus, the solution on the finest mesh is sufficiently precise to assess modelling errors accurately.

6 CONCLUSIONS

This paper shows that adaptive grid refinement can be used to create series of similar grids for convergence studies. Refining a coarse, unstructured hexahedral grid using a procedure based on metric tensors ensures that cells in all meshes have the same shapes and orientations, while the cell sizes in a mesh are proportional to the global refinement threshold T_r. Despite the limitation that the cells can only be divided in powers of two, the tests show that acceptable series of meshes are produced.

The computed forces were analysed with a standard uncertainty estimation technique. While some oscillations appear in the force convergence, the uncertainty estimations produce sensible results, which means that the series of meshes are suitable for this analysis. The convergence of local flow features, studied by visual inspection of isoline plots, is good. For the two-dimensional airfoil, the computed wake on the finest grids is identical, even far behind the trailing edge. In the more complicated flow around the KVLCC2, the velocity and the turbulence are nearly identical on the finest grids; the differences are small with respect to the distance between computations and experiments.

An advantage of adaptive meshing for grid convergence studies is the simplicity of the approach. Once a first computation is set up, simulations on different meshes are obtained by changing only the refinement threshold. Furthermore, a grid convergence study is not expensive, since one is interested in the results on the finest grid. Therefore, with respect to a one-grid computation only coarser grids are added. In three dimensions, the computations on all coarser grids together need little more than half the time for the finest grid. Finally, unstructured grids can be used without added difficulty. Thus, grid adaptation could make convergence studies accessible for everyday CFD simulation.

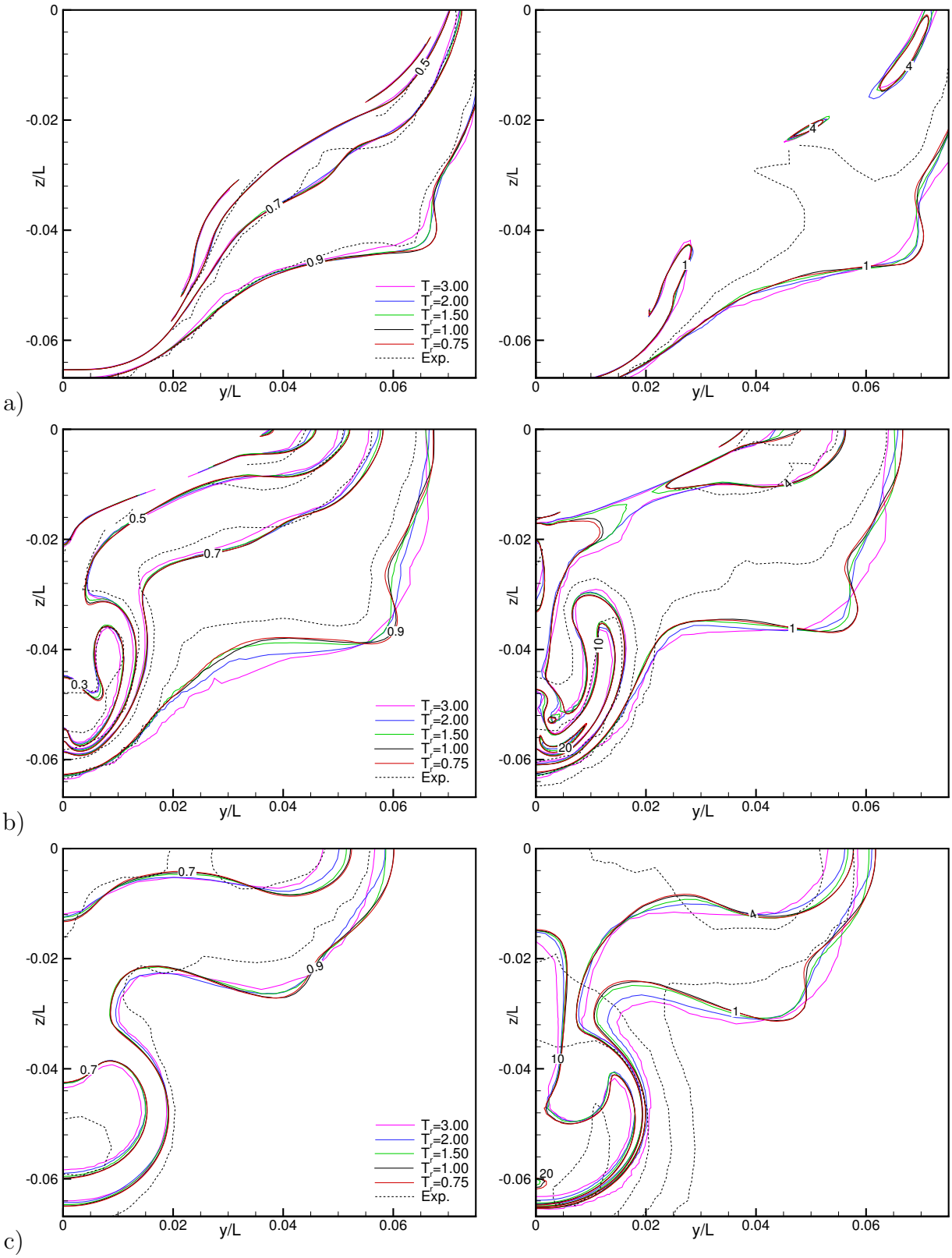

Figure 8: Grid convergence for the KVLCC2 in cut planes at $x/L = 0.9$ (a), in the propeller plane $x/L = 0.9825$ (b), and behind the ship at $x/L = 1.1$ (c): axial velocity (left) and turbulence kinetic energy (right).

ACKNOWLEDGEMENT

This work was granted access to HPC resources under the allocation 2015-2a1308 made by GENCI (Grand Equipement National de Calcul Intensif), which is gratefully acknowledged.

REFERENCES

[1] Wackers, J., Deng, G.B., Guilmineau, E., Leroyer, A., Queutey, P., Visonneau, M., Palmieri, A. and Liverani, A. Can adaptive grid refinement produce grid-independent solutions for incompressible flows? *J. Comput. Phys.* (2017) **344**:364–380.

[2] Wackers, J., Deng, G.B., Guilmineau, E., Leroyer, A., Queutey, P. and Visonneau, M. Combined refinement criteria for anisotropic grid refinement in free-surface flow simulation. *Comput Fluids* (2014) **55**:209–222.

[3] George, P.L. and Borouchaki, H. *Delaunay Triangulation and Meshing – Application to Finite Elements*. Hermes, 1998.

[4] Eça, L. and Hoekstra, M. A procedure for the estimation of the numerical uncertainty of CFD calculations based on grid refinement studies. *J. Comput. Phys.* (2014) **262**:104–130.

[5] Duvigneau, R., Visonneau, M. and Deng, G.B. On the role played by turbulence closures in hull shape optimization at model and full scale. *J. Mar. Sci. Techn.* (2003) **8**(1):1–25.

[6] Queutey P. and Visonneau, M. An interface capturing method for free-surface hydrodynamic flows. *Comput. Fluids* (2007) **36**(9):1481–1510.

[7] Nakayama, A. Characteristics of the flow around conventional and supercritical airfoils. *J. Fluid Mech.* (1985) **160**:155–179.

[8] Larsson, L., Stern, F., and Visonneau M. (eds.). *Numerical Ship Hydrodynamics, An assessment of the Gothenburg 2010 Workshop*. Springer (2014).